Heliyon 10 (2024) e29253

Contents lists available at ScienceDirect

Heliyon

journal homepage: www.cell.com/heliyon

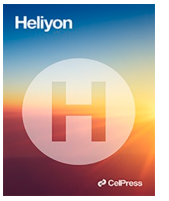

Research article

Flow field analysis of cigarette filter through micro-CT-based geometries and CFD simulation

Yunfei Song [a,1], Zixuan Liu [b,1], Zhiwei Sun [c,**], Wen Du [c], Zhiguo Wang [c], Zhigang Hu [b], Ming Ma [b,*], Zhiyong Wang [b]

[a] The Institute of Technological Sciences, Wuhan University, Wuhan, 430072, China
[b] School of Mechanical Engineering, Wuhan Polytechnical University, Wuhan, 430048, China
[c] Technology Center of China Tobacco Hunan Industrial Co., Ltd., Changsha, 410007, China

ARTICLE INFO

Keywords:
Micro-CT reverse engineering
Computational fluid dynamics
Cigarette filter
Wrapped paper
Porous media
Flue gas

ABSTRACT

The cigarette filter is an essential component of modern cigarettes and studying the flow distribution within the cigarette filter is of great significance in reducing the harm of cigarettes and optimizing smoking sensations. As the object of numerical simulation research, a three-dimensional model of the cigarette was accurately constructed through micro-CT reverse engineering, achieving a scanning accuracy of 4.05 μm. An overall porous media model of the cigarette filter was established to characterize the pressure distribution inside the filter. Based on the three-dimensional reconstruction, a local simulation model of the cavity-filtered filter was created by extracting a 1/36 geometric model. The simulation results of the overall porous media model of the cigarette filter were used as the pressure boundary conditions for the local simulation model of the cavity-filtered filter, and the effects of the wrapped paper and cavity on the flow field were analyzed. The results show that the simulated pressure drop in the overall porous media model of the cigarette filter had a deviation of less than 3.5% compared to the experimental results. This suggests that the porous media model can effectively predict the changes in pressure drop within the filter. When both wrapped paper and cavity were present, the velocity at the interface between acetate fiber and wrapped paper increased by 141.54%, while the pressure approached 0 Pa. Similarly, at the interface between acetate fiber and cavity, the velocity increased by 130.77%. It indicates that both wrapped paper and cavity significantly influenced the flow field characteristics within the cigarette filter. Additionally, as the porosity of the wrapped paper gradually increased from 0.69 to 0.99 in the radial direction, the fluid velocity increased by 14.46%, while the fluid pressure decreased by 29.09%. These changes were particularly evident when the porosity was below 0.87.

1. Introduction

With the advancement of research on smoking and health, it has been established that smoking is closely associated with various

* Corresponding author.
** Corresponding author.
E-mail addresses: sunzhw0327@hngytobacco.com (Z. Sun), maming@whpu.edu.cn (M. Ma).
[1] Co-first authors.

https://doi.org/10.1016/j.heliyon.2024.e29253
Received 15 October 2023; Received in revised form 17 February 2024; Accepted 3 April 2024
Available online 4 April 2024

diseases in humans. The study conducted by Belanger et al. [1] reveals that smoking is linked to an increased risk of tuberculosis. Saha et al. [2] have also highlighted that smoking significantly elevates the risk of cancer and cardiovascular diseases. Cigarette filters, which are essential components of modern cigarettes, reduce the presence of harmful substances in cigarette smoke and enhance the overall smoking experience. Hence, it is crucial to explore the flow distribution within cigarette filters to minimize the harmful effects of smoking and optimize the smoking experience.

Several researchers have employed fluid mechanics analysis to investigate the velocity, pressure, and other physical parameters of filter fibers or other fiber materials. Rostami et al. [3] developed a two-dimensional model to investigate the radial diffusion and axial convection of gas in porous media, specifically focusing on the diffusion process of CO and other gaseous smoke components through cigarette paper. Saidi et al. [4] created a model to study cigarette smoking and smoldering, exploring velocity and pressure distributions within the model, as well as mass flow through the ventilated sparse areas surrounding the paper and tobacco. Jaganathan et al. [5] employed digital volume imaging to analyze the complex microstructure of fibers, determining the permeability of the fiber microstructure through fluid flow simulation and obtaining velocity and pressure distributions in the fiber medium. Eitzinger et al. [6] developed a three-dimensional model for simulating smoking, allowing for flexible choices, and predicted the pressure, flow velocity, temperature, and gas concentration both inside and outside the cigarette. Hosseini et al. [7,8] constructed real 2D and 3D fiber filter media using C++ subroutines simulating particle filtration through Fluent's DPM, and obtaining the pressure drop in the fiber filter. Qian et al. [9] reconstructed a three-dimensional model of fiber media using SEM scanning and investigated the influence of fiber media structural parameters on pressure drop filtration efficiency, particle deposition, and aggregation by utilizing a CFD-DEM coupling method. Du et al. [10] optimized a theoretical model for cylindrical cigarette filter fibers to predict the smoke filtration efficiency of cigarette filters. Sun et al. [11] established a CFD model of Y-shaped filter fibers, simulating the velocity and pressure curves of smoke or nicotine particles within the filter, as well as the volume fraction curve of nicotine particles. In summary, the existing cigarette models developed by researchers have primarily focused on specific aspects, lacking a high-resolution physical model as a foundation for comprehensive simulation. Furthermore, as a novel filter variant, cavity filters have the potential to improve the smoking experience while effectively removing harmful components from smoke when compared to conventional filters. Nevertheless, research on this topic remains limited.

In the last decade, the use of high-resolution X-ray CT scanning has become increasingly popular for the 3D characterization of materials [12,13]. Gaiselmann et al. [14] introduced a segmentation algorithm capable of automatically extracting individual fibers from three-dimensional chromatographic data of fiber wirelessly. This algorithm was specifically applied to analyze a nonwoven material employed in the gas diffusion layer of polymer electrolyte membrane fuel cells. Thibault et al. [15] utilized X-ray micro-CT to reconstruct the structure of a felt material and characterized its structural parameters. Similarly, Badel et al. [16] conducted X-ray tomography to obtain experimental data on both the undeformed and deformed three-dimensional geometry of a fabric-reinforced material. They also assessed the fiber distribution in the yarn and compared the deformed geometry resulting from biaxial tensile and in-plane shear deformation, utilizing mesoscopic simulation and tomography. Zeng et al. [17] employed micro-CT tomography and image analysis to quantify the geometric parameters of the fabric. They conducted CFD simulation and static analysis to predict the in-plane permeability and tensile properties of the composite materials produced from the fabric. Straumit et al. [18] proposed a method to quantify the internal structure of textile composites and generate voxel models automatically based on X-ray CT tomography data. Amiot et al. [19] established a model for nonwoven using X-ray tomography and image analysis and investigated the tensile properties, compressibility, and air permeability of the nonwoven material. Meftah et al. [20] characterized the pore structure and acoustic properties of glass wool using a combination of X-ray micro-CT and simulation, enabling the non-destructive acquisition of quantitative 3D information regarding the internal pore network and fiber characteristics of glass wool. Tang et al. [21] employed reverse engineering to construct a three-dimensional model of the cigarette filter component and predicted the velocity, temperature, and pressure distribution of cigarette smoke at different time points.

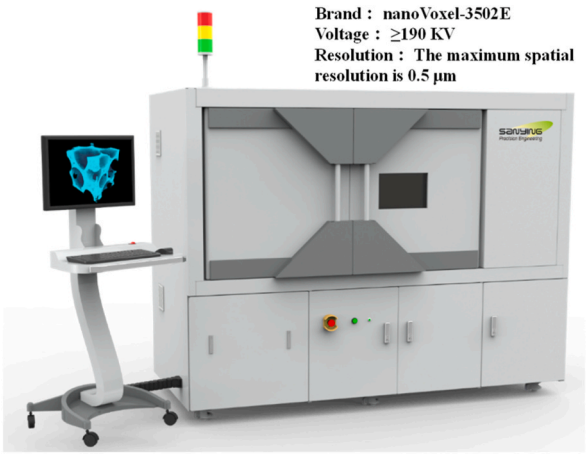

Fig. 1. NanoVoxel 3502E open-tube transmission high-resolution CT system.

This study utilizes a porous media approach to construct a comprehensive dimensional model of the cigarette filter, allowing for the analysis of pressure distribution within the filter. The model's accuracy is validated through pressure drop experiments. Additionally, a localized simulation model of the cavity filter is developed using micro-CT reverse engineering. This model enables the simulation of pressure and velocity distribution in the cigarette filter under various scenarios and the exploration of the impact of wrapped paper and cavity on the flow field. Furthermore, the influence of wrapped paper porosity on the flow field of the cavity filter is investigated by varying both the porosity and the corresponding viscosity and inertia resistance coefficients.

2. Material and methods

2.1. Micro-CT reverse engineering

This study used the nanoVoxel 3502E open-tube transmission high-resolution CT system provided by Tianjin Sanying Precision Instrument Company Limited in China (Fig. 1). The system operates at 80 kV and has a pixel matrix of 1920 × 1536. It can accommodate a maximum testable sample size of 450 mm × 350 mm and offers a remarkable resolution capability of 0.5 μm. The scanning accuracy utilized in this study is 4.05 μm. For the process of geometric reverse modelling, the study employed a method that involved segmenting the local filter model to obtain the geometric model of the local filter. The flowchart of the geometric extraction process for the local filter model is depicted in Fig. 2.

Geomagic Design X (Geomagic Design X 2020, Geomagic, Rock Hill, NC) and Geomagic Wrap (Geomagic Wrap 2021, Geomagic, Rock Hill, NC), which are two industrial modelling software, were utilized for geometric restoration and reconstruction based on the extracted point cloud STL model. The surface model of the cigarette filter and the interior acetate fiber were converted into a three-dimensional solid CAD model to simplify the overall model. The acetate fiber was divided into 1/4 to 1/36 parts for easier handling. In

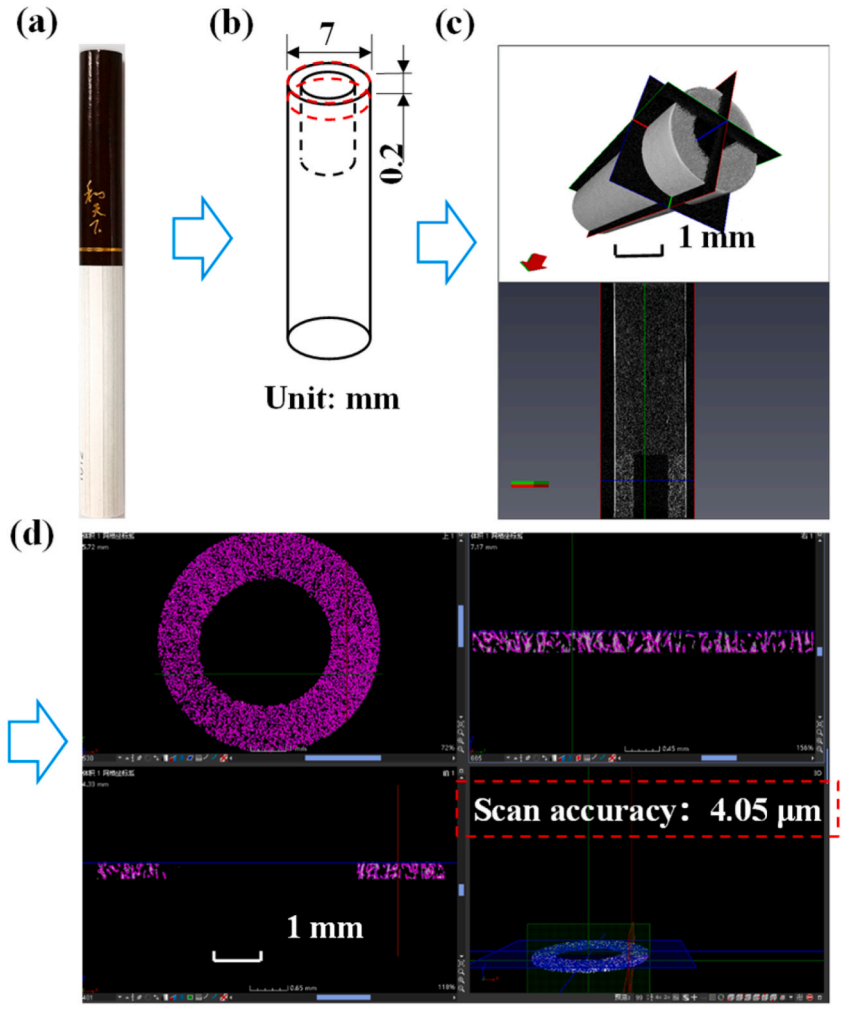

Fig. 2. (a) Cigarette samples, (b) geometric modeling of cigarette filter, (c) Micro-CT point cloud model of cigarette filter, and (d) geometric extraction of cavity filters.

order to reduce computational costs, the 1/36 geometric model was selected as the flow field simulation model. Fig. 3 illustrates the local geometric model of the acetate fiber.

2.2. Simulation modelling

To obtain the boundary conditions for the local simulation model, the overall cigarette filter simulation model was constructed. Polyhedral meshes were employed to ensure mesh quality and minimize the number of elements, creating a overall cavity filter model. Three boundary layers were applied to the wall and interface. The cavity filter meshes consisted of a total of 42,276,962 elements and 8,830,243 nodes. Fig. 4 illustrates the geometric and mesh models of the overall cavity filter.

To analyze the impact of paper wrapping and the cavity on the flow field, local filter simulation models were constructed for two scenarios: one without wrapped paper and the cavity, and the other considering wrapped paper and the cavity. Using the 1/36 local filter model, a Boolean operation was performed by embedding a fluid domain, resulting in a fluid domain for the fiber section. To enhance mesh quality, tetrahedral meshes were employed to generate a local filter mesh model, with three boundary layers applied to the wall and interface. The number of local filter-meshes, excluding the cavity, was 4,197,096, comprising 1,040,420 nodes. When considering the cavity, the number of local cavities filter meshes was 3,005,848, with 732,012 nodes. Fig. 5 illustrates both the local filter model and the mesh model, with and without considering wrapped paper and the cavity.

In this study, CFD was conducted using the ANSYS Fluent software (Fluent 2022 R1, ANSYS, Canonsburg, PA). A 3D transient simulation was performed to simulate the pressure and velocity changes in the cavity filter. As the flue gas was treated as an incompressible fluid, the Pressure-Based solver was used for the simulations. The Reynolds number calculated based on the flow velocity at the filter inlet, was found to be below 2300, indicating a laminar flow of smoke within the filter. Hence, the laminar model was chosen for the simulation calculations. Furthermore, to address any potential errors arising from the micro-CT and geometric reverse modelling processes, which could affect the accuracy of the fiber model, this study introduced the porous medium model. The fluid domain was designed as a porous medium to enhance authenticity and minimize errors.

In this study, the velocity-pressure coupling method utilized the SIMPLE algorithm, which calculated the pressure field based on a staggered grid to solve the momentum equation. To ensure accurate calculations, the gradient term was discretized using the Least-Squares Cell-Based method, which effectively prevented artificial diffusion. The discretization of the pressure term was done using the PRESTO method. Furthermore, a second-order upwind scheme was employed for the momentum equation to improve the reliability and accuracy of the simulation. To ensure accurate and precise calculation, the continuity equation and the convergence limit for the residual of each component were set to 10^{-6}.

2.3. Conservation equation

To simulate the flow of smoke in the cigarette, a species transport model was implemented, which adhered to the general conservation equations. The mass conservation equation [22] is depicted in Eq. (1).

$$\partial(\rho) / \partial t + \nabla \cdot (\rho \vec{v}) = 0 \tag{1}$$

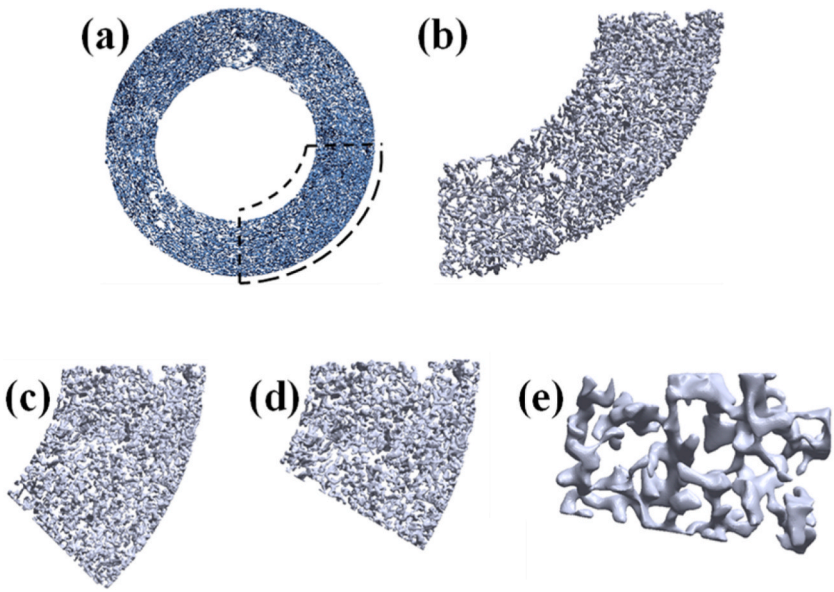

Fig. 3. Local geometric model of acetate fibers: (a) overall model, (b) 1/4 model, (c) 1/8 model, (d) 1/16 model, and (e) 1/36 model.

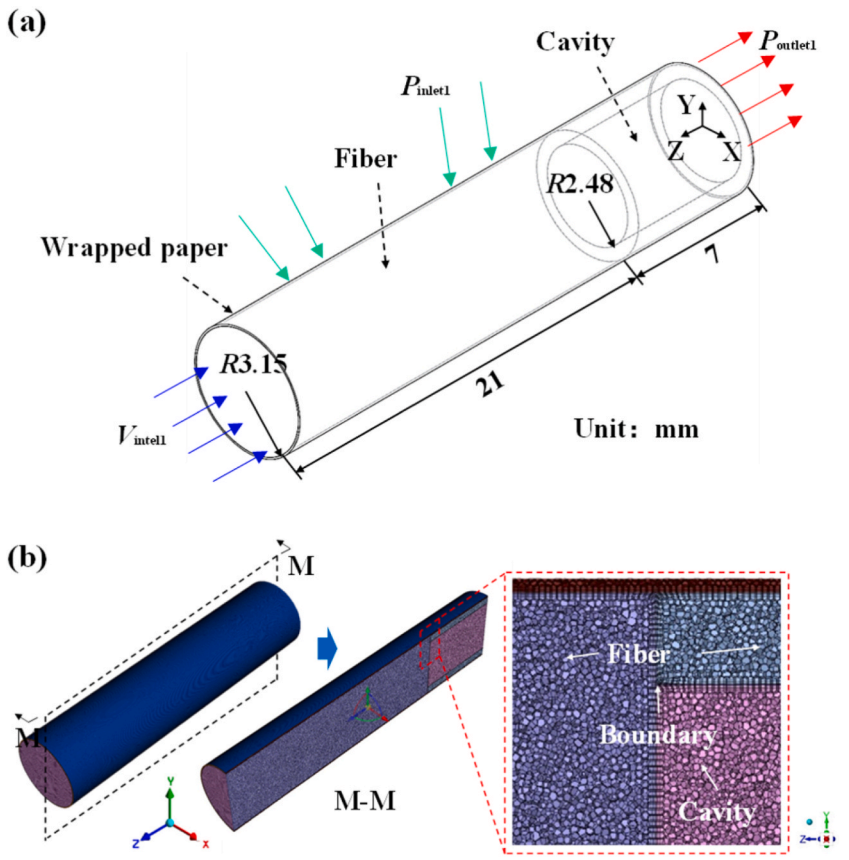

Fig. 4. (a) Geometric model and (b) finite element model of the overall cavity filter.

where ρ is the physical density, $\overrightarrow{v}$ is the velocity of the species.

The momentum conservation equation [22] is displayed in Eq. (2).

$$\partial(\rho\overrightarrow{v})/\partial t+\nabla\cdot(\rho\overrightarrow{v}\overrightarrow{v})=-\nabla p+\nabla\cdot(\mu\nabla\overrightarrow{v})+\rho\overrightarrow{g} \tag{2}$$

where p is the phase of stress tensor in fluid, $\rho\overrightarrow{g}$ is the gravity volume force, μ is the molecular viscosity.

2.4. Boundary condition

In the overall cavity filter model, the wrapped paper and acetate parts were defined as porous media when configuring the fluid domain. Based on international standards published by ISO [23], the volume flow rate of the standard flue gas is 17.5 mL/s, and the corresponding velocity is 0.56 m/s. Table 1 illustrates the simulation boundary conditions for the flow field of the complete cavity filter. In addition, the two cross-sections of the model along the radial direction are defined to be symmetric.

The study established simulation boundary conditions for the 1/36 local filter model of the cavity filter, which had a thickness of 0.22 mm. The pressure outlet was set at $Z=0$ mm with a value of $P_{outlet2,3}=-550$ Pa, while the pressure inlet was set at $Z=0.22$ mm. The pressure inlet for the 1/36 local filter model of the cavity filter was determined separately for two parts: the cavity and the acetate fiber. In the cavity part, the pressure was maintained uniformly, and the root mean square was calculated and averaged as shown in Eq. (3). However, since the pressure at the acetate fiber exhibited significant variation, a weighted average was taken into consideration, as shown in Eq. (4).

$$P_{inlet3}=-P_{\mathrm{rms}}=-\sqrt{1\Big/\mathrm{N}\sum_{1}^{i}P_i^2} \tag{3}$$

$$P_{inlet2,4}=\overline{P}=(P_1w_1+P_2w_2+\ldots+P_iw)/(w_1+w_2+\ldots+w_i) \tag{4}$$

in the local fiber mesh model, the cavity serves was designated as the flue gas domain, while the wrapped paper was modelled as a porous medium with a porosity of 0.9. The entire surface of the wrapped paper was designated as a pressure inlet, enabling the cooling

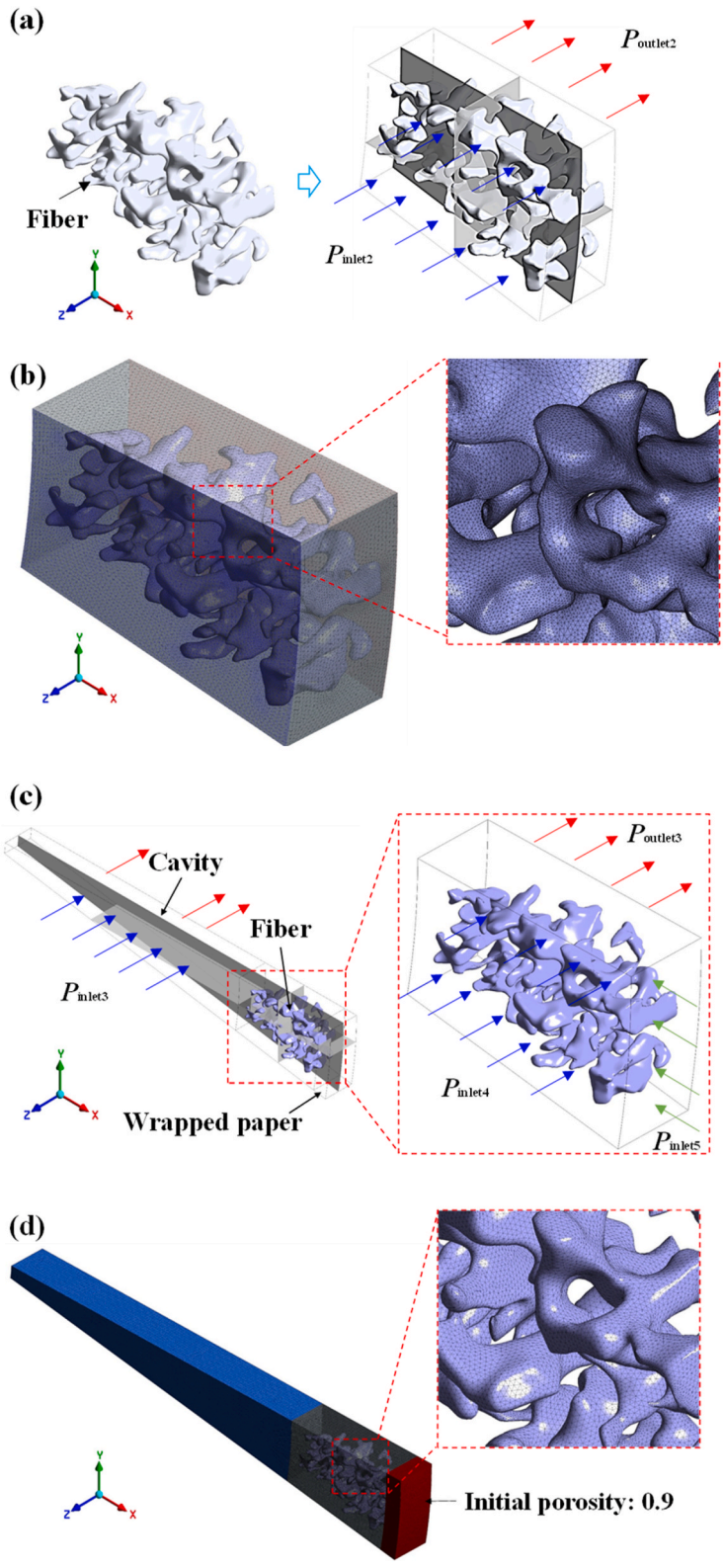

Fig. 5. Local filter (a) geometric model and (b) finite element model without considering wrapped paper and cavity and (c) geometric model and (d) finite element model with considering wrapped paper and cavity.

Table 1
Simulation boundary conditions for the overall cigarette cavity filter model with porous media.

Boundary/fluid domain	Parameter setting	
$\boldsymbol{V}_{\text{inlet1}}$	Velocity: 0.56 m/s	Temperature: 500 K
$\boldsymbol{P}_{\text{intet1}}$	Pressure: 0 Pa	Temperature: 300 K
$\boldsymbol{P}_{\text{outlet1}}$	Pressure: −550 Pa	Temperature: 300 K
Wall surface	Temperature: 300 K	
Fluid domain (acetate fiber)	Porosity: 0.77	
	Viscous resistance coefficient: 2.86exp + 9	
	Inertial resistance coefficient: 7.49exp + 4	
Fluid domain (wrapped paper)	Porosity: 0.9	
	Viscous resistance coefficient: 3.42exp + 8	
	Inertial resistance coefficient: 2.04exp + 4	

of the mainstream flue gas. The pressure at the inlet was set to $P_{\text{inlet5}} = 0$ Pa.

When the porosity of the wrapped paper varied, the viscous and inertial resistance coefficients could be determined using the Forchheimer flow resistance model [24], as depicted in Eq. (5), and the Ergun equation [24], as represented by Eq. (6).

$$\Delta P \Big/ L = av + bv^2 \tag{5}$$

$$\Delta P \Big/ L = A\left[(1-\varepsilon)^2 \mu \Big/ \varepsilon^3 d_p^2\right] v + B\left[(1-\varepsilon) \Big/ \varepsilon^3 d_p\right] p v^2 \tag{6}$$

2.5. Experimental methodology

This study conducted an experiment to measure the suction resistance of a fiber filter. The test sample comprised four cigarette fiber filters together. The suction resistance of gas flowing through the fiber filter was measured using the DT-S modular testing station provided by Borgwaldt KC GmbH in Germany, as shown in Fig. 6.

When the fiber medium complied with the Darcy's law, it must also obey the following Eq. (7), where the left term represented the Darcy's law.

$$\Delta P A d_f^2 \Big/ \mu V H = f(\alpha) \tag{7}$$

where A represents the cross-sectional area of the fiber, d_f represents the fiber diameter, μ represents the gas viscosity, V represents the apparent filtration velocity, α represents the filling rate, and ΔP represents the pressure drop caused by gas flowing through the fiber medium.

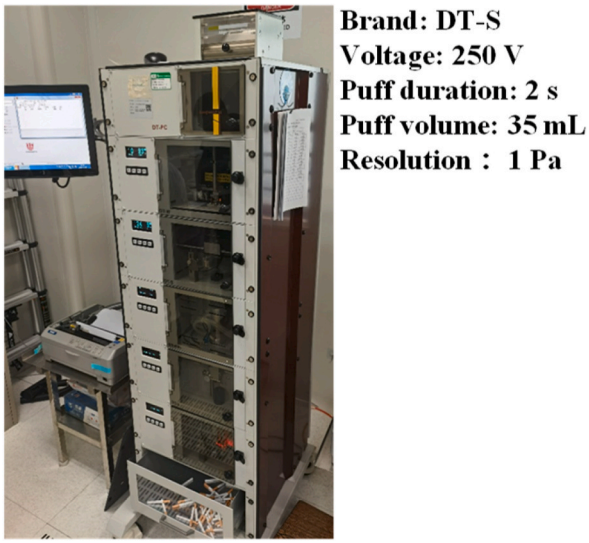

Fig. 6. DT-S modular testing station.

3. Results and discussion

3.1. Pressure drop in the overall cavity filter

This study characterized the velocity and pressure distribution inside the filter based on the overall porous media model of the cigarette filter to obtain the boundary conditions for the local simulation model.

Fig. 7 depicts contour maps that illustrate the distribution of velocity and pressure within the filter cavity. As shown in Fig. 7(a), the mainstream smoke maintained a velocity of approximately 0.56 m/s in the acetate fiber region. Near the wrapped paper, the mainstream smoke was influenced by external airflow, which entered the fibers and diffused along with the mainstream smoke toward the outlet. Within the cavity, where there was no flow resistance, the velocity gradually increased to 10 m/s. The internal smoke within the fibers near the cavity was primarily affected by the ventilation airflow and the cavity itself, leading to some of the mainstream smoke overflowing into the cavity. As depicted in Fig. 7(b), the pressure distribution was observed in the acetate fiber. Close to the wrapped paper, the pressure approached 0 Pa due to the impact of external airflow. Inside the cavity, without flow resistance, the pressure gradually decreased from −200 Pa at the bottom of the cavity to −550 Pa at the outlet.

The axial pressure distribution at different radial positions was obtained from the cloud diagram illustrating the axial pressure distribution in the cavity filter model. The resulting curve of axial pressure variation with radius was plotted (Fig. 8). The pressure distribution in the acetate fiber varied at different positions due to the impact of ventilation airflow from the wrapped paper. At various radial positions, the pressure in the acetate fiber gradually decreased and then rapidly dropped to −550 Pa near the pressure outlet ($Z = 0$ to $Z = 1$ mm). In contrast, the pressure variation in the cavity along the axial direction appeared to be consistent at different radial positions, gradually decreasing from −200 Pa to −550 Pa. This can be attributed to the fact that the cavity section was only primarily influenced by the overflow of internal smoke from the acetate fiber, resulting in a relatively stable pressure distribution.

Similarly, the radial pressure distribution at different horizontal positions was obtained from the cloud diagram illustrating the axial pressure distribution in the cavity filter model. The resulting curve, illustrating the radial pressure variation with a horizontal position is presented in Fig. 9. Within the acetate fiber, the fluid pressure gradually increased to 0 Pa along the radial direction, while the fluid pressure in the cavity region remained constant. This can be attributed to the impact of the external airflow on the mainstream smoke near the wrapped paper, causing the observed pressure variations.

Fig. 10 shows a comparison between the experimental and simulation results of the pressure drop in the overall cavity filter. When the flue gas, with an average molecular diameter of 0.4 μm, passed through the fiber filter at a flow rate of 0.56 m/s, the pressure drop of the flue gas was measured and recorded to compare with the simulation result of the overall porous media model of the cigarette filter. The pressure drop of the simulation across the 21 mm long fiber filters was $\Delta P = 544.57$ Pa, while the pressure drop values for the three sample groups were approximately 2219.33 Pa with an overall error of less than 3%. The pressure drop curve closely followed Darcy's law, with a deviation of less than 3.5% when compared to the experimental results. Therefore, the proposed research model demonstrated enhanced accuracy in predicting variations in pressure drop within the filter.

Fig. 11 presents the changes in radial pressure at $Z = 0.22$ mm in the overall cigarette filter model, which corresponds to the entrance cross-section of the local filter model. The pressure in the cavity part remains uniform, ranging from −550 Pa to −500 Pa. However, the pressure at the acetate fiber varied significantly, increasing from −500 Pa to nearly 0 Pa as the radius increases.

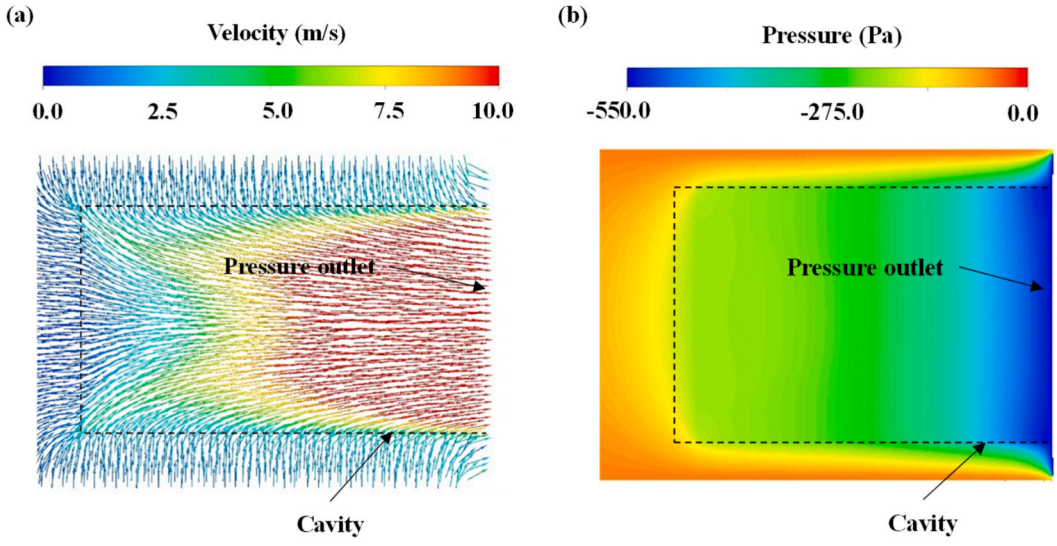

Fig. 7. Nephogram depicting the axial distribution of (a) velocity and (b) pressure in the overall cavity filter.

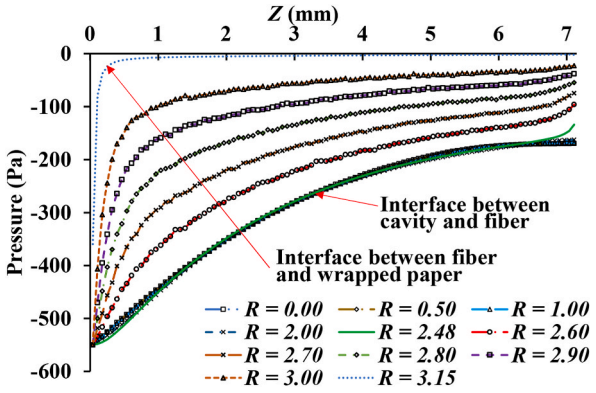

Fig. 8. Changes in axial pressure at different radius positions in the overall cavity filter.

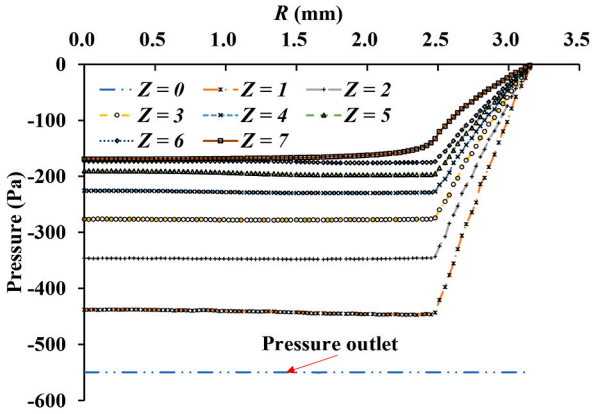

Fig. 9. Changes in radial pressure at different horizontal positions in the overall cavity filter.

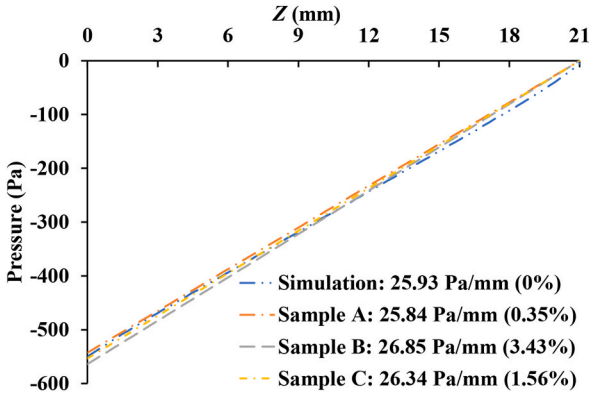

Fig. 10. Comparison of the experimental and simulation results for the pressure drop in the overall cavity filter.

3.2. Effect of cavity and wrapped paper on the flow field in the local cigarette filter

The local cigarette filter model depicted in Fig. 5 was simulated using the boundary conditions obtained from the overall cavity filter model simulation. Based on the simulation results of the overall cavity filter in Fig. 11, the boundary conditions for the pressure inlet of the local filter model were calculated using Eq. (3) and Eq. (4). The pressure in the cavity part was $P_{\text{inlet3}} = -527.5$ Pa, while the pressure at the acetate fiber was $P_{\text{inlet2,4}} = -313.0$ Pa. The boundary conditions were illustrated in Table 2.

Fig. 12 illustrates the velocity distribution nephogram with and without considering ventilation and the cavity. When both the wrapped paper and the cavity were present, the velocity at the interface between the acetate fiber and the wrapped paper increased by

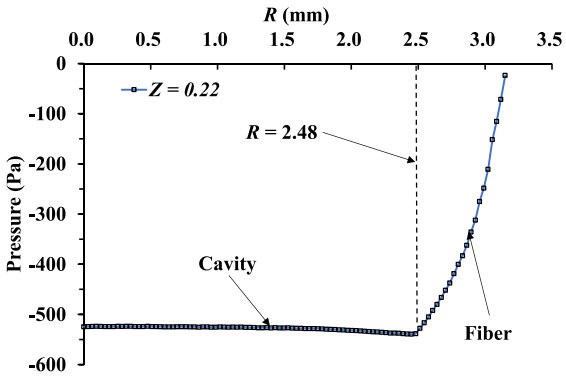

Fig. 11. Changes in radial pressure at $Z = 0.22$ mm in the overall cavity filter.

Table 2
Simulation boundary conditions for the local cigarette filter model with porous media.

Boundary/fluid domain	Parameter setting	
P_{inlet2}	Pressure: −527.5 Pa	Temperature: 500 K
P_{inlet3}	Pressure: −313.0 Pa	Temperature: 500 K
P_{inlet4}	Pressure: −527.5 Pa	Temperature: 500 K
P_{inlet5}	Pressure: 0 Pa	Temperature: 300 K
$P_{outlet2}$	Pressure: −550.0 Pa	Temperature: 300 K
$P_{outlet3}$	Pressure: −550.0 Pa	Temperature: 300 K
Wall surface	Temperature: 300 K	
Fluid domain (acetate fiber)	Porosity: 0.77	
	Viscous resistance coefficient: 2.86exp + 9	
	Inertial resistance coefficient: 7.49exp + 4	
Fluid domain (wrapped paper)	Porosity: 0.9	
	Viscous resistance coefficient: 3.42exp + 8	
	Inertial resistance coefficient: 2.04exp + 4	

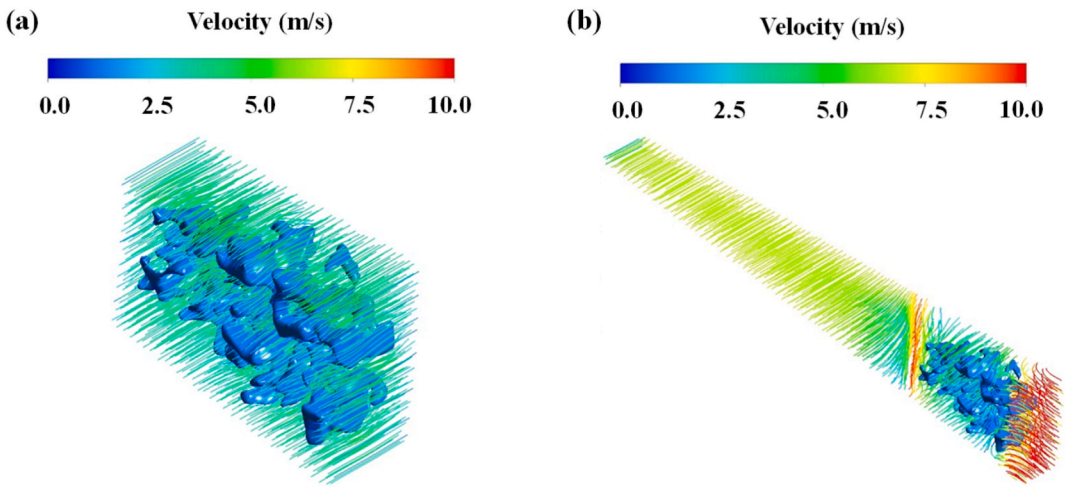

Fig. 12. Cloud diagrams depicting velocity distribution under two scenarios: (a) without considering ventilation and cavity, (b) with considering ventilation and cavity.

141.54% than that without considering the wrapped paper and cavity, while the velocity at the interface between the acetate fiber and the cavity increased by 130.77%.

When the influence of the cavity and ventilation was not taken into account, the main flue gas was primarily impeded by the acetate fiber, resulting in local disturbances. However, when considering the influence of the cavity and ventilation, the main flue gas was affected by various factors, including the acetate fiber, cavity, and wrapped paper. The acetate fiber continued to hinder the local

disturbances in the flow of the main flue gas, similar to the previous scenario. Since there was no flow resistance in the cavity, a portion of the flue gas in the intersection area between the acetate fiber and the cavity spilled into the cavity and was discharged along with the flue gas within it. The airflow within the wrapped paper was perpendicular to the mainstream flue gas, and as it approached the wrapped paper, the impact of the mainstream flue gas in the area of the acetate fiber became more pronounced, resulting in more noticeable disturbances.

Fig. 13 illustrates the pressure distribution nephogram under two scenarios: without considering ventilation and cavity, and with ventilation and cavity taken into account. When comparing the results of the flow field, it can be observed that the pressure on the surface of the acetate fiber remained largely consistent in most areas. However, when ventilation was introduced, the pressure at the interface between the acetate fiber and the wrapped paper approached 0 Pa. The vertical impact of external airflow on the mainstream smoke had a significant effect on the flow field near the wrapped paper. As a result, the presence of the cavity and the wrapped paper significantly influences the flow field characteristics within the filter.

3.3. *Effect of the porosity of the wrapped paper on the flow field in the local cigarette filter*

The higher porosity of the wrapped paper enhances air permeability, resulting in increased air absorption during inhalation. This reduces airflow through the cigarette's burning end, leading to decreased tobacco combustion and, consequently, a reduction in the inhalation of tar. Therefore, exploring an appropriate porosity level for wrapped paper is crucial.

By adjusting the porosity of the wrapped paper and its corresponding viscous resistance coefficient and inertial resistance coefficient, the impact of changes in the porosity of the wrapped paper on the flow field was further investigated. Based on Eq. (5) and Eq. (6), the viscosity and inertia resistance coefficients corresponding to different porosities were provided in Table 3, while other parameters were kept unchanged as listed in Table 2.

Fig. 14 illustrates the distribution of fluid velocity along the radial direction for different porosities of the wrapped paper. In the presence of external air perpendicular to the mainstream flue gas within the wrapped paper, it affected the flow dynamics. Consequently, the fluid velocity increased as the radial position increased and eventually stabilizes. Furthermore, at the same radial position, the fluid velocity gradually increased with the higher porosity of the wrapped paper. Particularly, when the porosity was below 0.87, the fluid velocity exhibited more noticeable variations with the porosity. The average change rate of fluid velocity between adjacent porosities exceeded 1%, reaching a maximum of 2.34%. However, for porosities above 0.87, the fluid velocity showed less sensitivity to changes in porosity. The average change rate of fluid velocity between adjacent porosities was less than 1%, with a minimum of 0.47%. This behavior could be attributed to the influence of porosity on viscous resistance and inertial resistance, as indicated in Table 3. Smaller porosities have a greater impact on these resistances, resulting in more significant effects on fluid velocity.

Fig. 15 illustrates the distribution of fluid pressure along the radial direction for different porosities of the wrapped paper. Within the wrapped paper, there was a mutual impact between the mainstream flue gas and external air. Consequently, the fluid pressure initially increased in the radial direction, then decreased with increasing radial position, and eventually stabilized. Furthermore, at the same radial position, the fluid pressure gradually decreased with the increasing porosity of the wrapped paper. Specifically, when the porosity was below 0.87, the fluid pressure exhibited more noticeable changes with the porosity. The average fluid pressure change rate between adjacent porosities exceeded 2%, reaching up to 4.38%. However, when the porosity was greater than 0.87, the fluid pressure changes less with the porosity. The average fluid pressure change rate between adjacent porosities was less than 2%, as low as 0.83%. This behavior was similar to the change in fluid velocity. Smaller porosities had a greater influence on viscous resistance and inertial resistance, resulting in a more pronounced effect on fluid pressure.

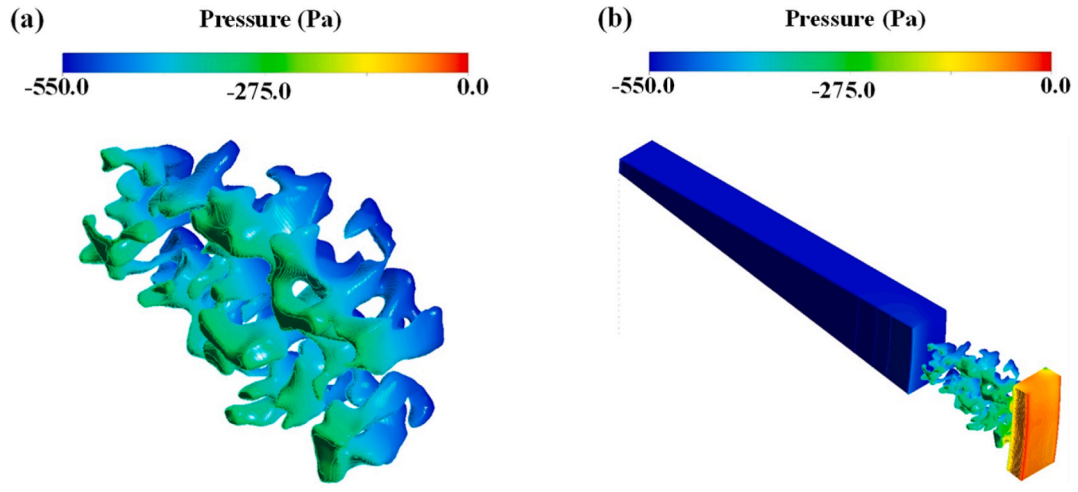

Fig. 13. Cloud diagram depicting pressure distribution under two scenarios: (a) without considering ventilation and cavity, (b)with considering ventilation and cavity.

Table 3
Viscosity and inertia resistance coefficients corresponding to porosity.

Porosity	Viscous resistance coefficient	Inertial resistance coefficient
0.69	7.30exp +9	1.40exp +5
0.72	5.24exp +9	1.12exp +5
0.75	3.69exp +9	8.81exp +4
0.78	2.54exp +9	6.89exp +4
0.81	1.69exp +9	5.32exp +4
0.84	1.08exp +9	4.01exp +4
0.87	6.40exp +8	2.94exp +4
0.9	3.42exp +8	2.04exp +4
0.93	1.52exp +8	1.29exp +4
0.96	4.51exp +7	6.72exp +3
0.99	2.57exp +6	1.53exp +3

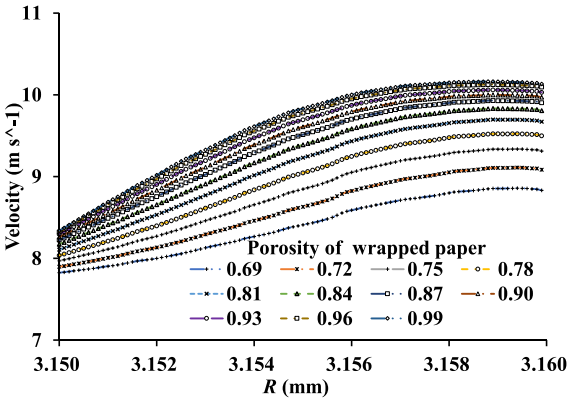

Fig. 14. Radial velocity distribution curve with different porosities of wrapped paper.

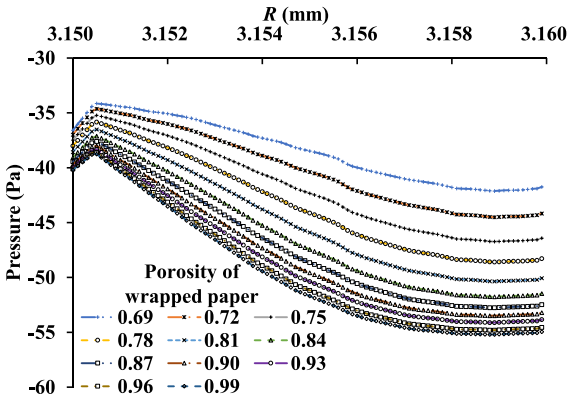

Fig. 15. Radial pressure distribution curve with different porosities of wrapped paper.

4. Conclusions

In this study, the flow field of cigarette filters was analyzed using micro-CT reverse engineering and CFD simulation. Firstly, a porous media approach was employed to construct an overall dimensional model of the cigarette filter. Secondly, the simulation results of the overall cavity filter porous media model were used as the pressure boundary conditions for a local filter model. This local model was created from a 1/36 geometric model obtained through micro-CT scanning, representing the local filter with a thickness of 0.22 mm. The aim was to investigate the effects of the wrapped paper and cavity on mainstream smoke. Finally, the velocity and pressure distribution at the interface between the fiber and wrapped paper were analyzed by adjusting the porosity of the wrapped paper and its corresponding viscous resistance coefficient and inertial resistance coefficient.

The results of the study indicated good consistency between the simulation results based on the porous media model and the

experimental data, with a deviation of less than 3.5%. Additionally, when both the wrapped paper and cavity were presented, there was an overflow of smoke into the cavity from the acetate fiber-cavity interface, resulting in a 130.77% increase in flow velocity. The acetate fiber-wrapped paper interface experienced disturbances from incoming air and mainstream smoke, leading to a 141.54% increase in flow velocity, and the pressure approached 0 Pa. These findings showed that both the wrapped paper and cavity significantly influenced the flow field characteristics within the cigarette filter. Furthermore, an increase in the porosity of the wrapped paper from 0.69 to 0.99 resulted in a 14.46% increase in fluid velocity in the radial direction and a 29.09% decrease in fluid pressure. Notably, when the porosity was below 0.87, the fluid velocity and pressure exhibited more noticeable changes with the porosity.

The findings of this study have practical implications for industries involved in cigarette filter design and manufacturing. By understanding the flow dynamics within cigarette filters, manufacturers can improve product performance, enhance filtration efficiency, and meet regulatory standards more effectively.

CRediT authorship contribution statement

Yunfei Song: Writing – original draft, Methodology, Formal analysis, Conceptualization. **Zixuan Liu:** Writing – original draft, Validation, Investigation. **Zhiwei Sun:** Supervision, Resources, Conceptualization. **Wen Du:** Supervision, Resources. **Zhiguo Wang:** Supervision. **Zhigang Hu:** Project administration. **Ming Ma:** Writing – review & editing, Project administration. **Zhiyong Wang:** Project administration.

Declaration of competing interest

The authors declare that they have no known competing financial interests or personal relationships that could have appeared to influence the work reported in this paper.

Acknowledgements

The numerical calculations in this paper have been done on the supercomputing system in the Supercomputing Center of Wuhan University. This work was also supported by the Opening Fund of Cigarette Functional Material/Digital and Intelligent Flavoring Key laboratory of China Tobacco (China Tobacco Hunan Industrial Co., Ltd.) (KY2022KF0006).

References

[1] K. Belanger, W. Beckett, E. Triche, M. Bracken, T. Holford, P. Ren, J. McSharry, D. Gold, T. Platts-Mills, B. Leaderer, Symptoms of wheeze and persistent cough in the first year of life: associations with indoor allergens, air contaminants, and maternal history of asthma, Am. J. Epidemiol. 158 (3) (2003) 195–202, https://doi.org/10.1093/aje/kwg148.
[2] S. Saha, D. Bhalla, T. Whayne, C. Gairola, Cigarette smoke and adverse health effects: an overview of research trends and future needs, Int. J. Angiol. 16 (3) (2007) 77–83, https://doi.org/10.1055/S-0031-1278254.
[3] A. Rostami, M. Hajaligol, Modeling the diffusion of carbon monoxide and other gases from the paper wrapper of a cigarette during puffing, J. Anal. Appl. Pyrol. 66 (2003) 263–280, https://doi.org/10.1016/S0165-2370%2802%2900154-7.
[4] M. Saidi, M. Hajaligol, F. Rasouli, Numerical simulation of a burning cigarette during puffing, J. Anal. Appl. Pyrol. 72 (2004) 141–152, https://doi.org/10.1016/J.JAAP.2004.03.011.
[5] S. Jaganathan, H. Tafreshi, B. Pourdeyhimi, A realistic approach for modeling permeability of fibrous media: 3-D imaging coupled with CFD simulation, Chem. Eng. Sci. 63 (2008) 244–252, https://doi.org/10.1016/J.CES.2007.09.020.
[6] B. Eitzinger, S. Pirker, Numerical simulation of a cigarette during smoking, Contributions to Tobacco & Nicotine Research 21 (7) (2005) 403–416, https://doi.org/10.2478/cttr-2013-0806.
[7] S.A. Hosseini, H. Tafreshi, Modeling particle filtration in disordered 2-D domains: a comparison with cell models, Separ. Purif. Technol. 74 (2010) 160–169, https://doi.org/10.1016/J.SEPPUR.2010.06.001.
[8] S.A. Hosseini, H. Tafreshi, 3-D simulation of particle filtration in electrospun nanofibrous filters, Powder Technol. 201 (2010) 153–160, https://doi.org/10.1016/J.POWTEC.2010.03.020.
[9] F. Qian, N. Huang, X. Zhu, J. Lu, Numerical study of the gas–solid flow characteristic of fibrous media based on SEM using CFD–DEM, Powder Technol. 249 (2013) 63–70, https://doi.org/10.1016/J.POWTEC.2013.07.030.
[10] W. Du, J. Wen, B. Peng, X. Zhang, Fuwei Xie, L. Huimin, K. Zhong, An improved theoretical model of cigarette smoke filtration across Mono-Segment cellulose acetate filters, Contributions to Tobacco & Nicotine Research 26 (5) (2015) 232–240, https://doi.org/10.1515/cttr-2015-0011.
[11] Z. Sun, J. Wen, X. Luo, W. Du, Z. Liang, K. Fu, An improved CFD model of gas flow and particle interception in a fiber material, Chin. J. Chem. Eng. 25 (2017) 264–273, https://doi.org/10.1016/J.CJCHE.2016.08.026.
[12] J. Buffière, E. Maire, J. Adrien, J. Masse, E. Boller, In situ experiments with X ray tomography: an attractive tool for experimental Mechanics, Exp. Mech. 50 (2010) 289–305, https://doi.org/10.1007/S11340-010-9333-7.
[13] H. Tran, P. Doumalin, C. Delisée, J. Dupré, J. Malvestio, A. Germaneau, 3D mechanical analysis of low-density wood-based fiberboards by X-ray microcomputed tomography and Digital Volume Correlation, J. Mater. Sci. 48 (2013) 3198–3212, https://doi.org/10.1007/s10853-012-7100-0.
[14] G. Gaiselmann, I. Manke, W. Lehnert, V. Schmidt, Extraction of curved fibers from 3D data, KIT Scientific Publishing 32 (2013) 57–63, https://doi.org/10.5566/IAS.V32.P57-63.
[15] X. Thibault, J. Bloch, Structural analysis by X-Ray microtomography of a strained nonwoven papermaker felt, Textil. Res. J. 72 (2002) 480–485, https://doi.org/10.1177/004051750207200603.
[16] P. Badel, E. Vidal-Sallé, E. Maire, P. Boisse, Simulation and tomography analysis of textile composite reinforcement deformation at the mesoscopic scale, Int. J. Material Form. 2 (2008) 189–192, https://doi.org/10.1016/J.COMPSCITECH.2008.04.038.
[17] X. Zeng, L. Brown, A. Endruweit, M. Matveev, A. Long, Geometrical modelling of 3D woven reinforcements for polymer composites: prediction of fabric permeability and composite mechanical properties, Compos. Appl. Sci. Manuf. 56 (2014) 150–160, https://doi.org/10.1016/J.COMPOSITESA.2013.10.004.
[18] I. Straumit, S. Lomov, M. Wevers, Quantification of the internal structure and automatic generation of voxel models of textile composites from X-ray computed tomography data, Compos. Appl. Sci. Manuf. 69 (2015) 150–158, https://doi.org/10.1016/J.COMPOSITESA.2014.11.016.
[19] M. Amiot, M. Lewandowski, P. Leite, M. Thomas, A. Perwuelz, An evaluation of fiber orientation and organization in nonwoven fabrics by tensile, air permeability and compression measurements, J. Mater. Sci. 49 (2013) 52–61, https://doi.org/10.1007/s10853-013-7323-8.

[20] R. Meftah, S. Berger, G. Jacqus, Jean-Yves Laluet, V. Cnudde, Multiscale characterization of glass wools using X-ray micro-CT, Mater. Char. 156 (2019) 109852, https://doi.org/10.1016/J.MATCHAR.2019.109852.
[21] D. Tang, J. Wu, J. Zeng, W. Gao, D. Liang, Research on cigarette during smoking based on reverse engineering and numerical simulation, Chin. J. Chem. Eng. 27 (10) (2019) 2359–2375, https://doi.org/10.1016/J.CJCHE.2019.04.020.
[22] Y. Sheng, M. Wang, L. Zhang, Q. Ren, Analysis of filtration process of 3-D mesh spacer filter by using CFD-DEM simulation, Powder Technol. 396 (2022) 785–793, https://doi.org/10.1016/j.powtec.2021.11.034.
[23] ISO 6565-2015, Tobacco and Tobacco Products - Draw Resistance of Cigarettes and Pressure Drop of Filter Rods - Standard Conditions and Measurement..
[24] S. Ergun, Fluid flow through packed columns, Chem. Eng. Prog. 48 (2) (1952) 89–94.